Independent yields from the photofission of ^{232}Th, and the Z_p and statistical-dynamic models

J. R. Smith* and A. E. Richardson†
Department of Chemistry, New Mexico State University, Las Cruces, New Mexico 88003
(Received 18 June 1990)

Independent fission yields were measured for ^{82}Br, ^{96}Nb, ^{124}Sb, and ^{126}Sb produced by photofission of ^{232}Th with 27-MeV peak bremsstrahlung and for ^{136}Cs at 11, 15, and 27 MeV. Upper limits for the independent yields for ^{86}Rb and ^{134}Cs and mass yields for mass chains 125 and 127 were also measured for ^{232}Th photofission at 27 MeV. Various extensions of the Z_p charge-distribution model were found to give generally good agreement with experimental measurements in the asymmetric mass regions, but less satisfactory agreement in the symmetric region. A statistical charge-distribution model incorporating post-fission dynamics correlated well with experimental values in both symmetric and asymmetric regions. The statistical-dynamic model naturally predicted pairing and shell effects which were in good agreement with experimentally observed effects. One important outcome of the statistical-dynamic model calculations was the production of a linear shape on the wings of the charge-distribution curve when proximity proton transfer after scission was incorporated into the model. Such linear shapes have previously been experimentally observed without explanation.

I. INTRODUCTION

Photofission reactions make use of the simplicity and directness of the electromagnetic interaction as a powerful tool with which to explore the process of nuclear fission [1]. Since much of the detail in fission yields, such as pairing and shell effects, is washed out at high excitation energies [2,3], the use of low-energy bremsstrahlung to induce fission will maximize the amount of information for fission dynamics that can be obtained from mass and charge distributions.

In recent years there has been renewed interest in low-energy bremsstrahlung-induced fission [4–7]. This is due, in part, to new data on photofission cross sections for ^{235}U, ^{236}U, ^{238}U, and ^{232}Th which were obtained using monoenergetic photons with energies from threshold to 18.3 MeV, an energy range that nearly covers that of the giant dipole resonance for these nuclei [8,9]. However, only limited data have been available on independent yields from bremsstrahlung-induced fission of ^{232}Th [10]. This scarcity of data was the main impetus for the present investigation.

In addition to obtaining independent yields, other objectives of this investigation were to determine fractional-independent yields (FIY's) and use these to evaluate various methods for calculating FIY's [11–15]. The main intent was to uncover some of the dynamics that led to the observed charge distributions. Special attention was paid to those methods which were developed around physical principles and less attention to those which were more empirical. A model has been developed which has added post-fission dynamics to the original statistical model of Fong [15]. We will call this model the statistical-dynamic model.

II. EXPERIMENT

40-g samples of reagent-grade $Th(NO_3)_4 \cdot 4H_2O$ in polyethylene ampoules were irradiated in the bremsstrahlung beam of the electron linear accelerator (LINAC) at the Nuclear Effects Directorate at White Sands Missile Range (WSMR). The duration of each irradiation was approximately 1 h with a pulse rate of 30 pulses per sec and a beam current of 200 mA. Three irradiations were performed with 27-MeV peak bremsstrahlung, one with 15 MeV, and one with 10 MeV.

The first step in obtaining the independent fission yields of ^{82}Br, ^{96}Nb, ^{86}Rb ^{124}Sb^g, ^{126}Sb^g, ^{134}Cs, and ^{136}Cs, and the mass yields of ^{125}Sb and ^{127}Sb, was to perform a chemical separation of each of the respective elements from successive weighed samples of irradiated $Th(NO_3)_4 \cdot 4H_2O$. In addition, a chemical separation of barium from approximately 1 g of the irradiated thorium nitrate was carried out so that all independent and mass yields could be normalized to the 7.81% mass yield of ^{140}Ba reported by Hogan *et al.* [6].

The procedures used for the chemical separations were developed from standard radiochemical methods [16–19]. The separation of barium was not changed from the standard method [16,17]. An initial step was added in each of the other procedures to remove most of the thorium from the reaction mixture which would otherwise have interfered with some of the steps in the separation procedures.

Some difficulty was encountered in performing the standard radiochemical procedure with niobium [16]. It was found that fission-product niobium was not oxidized to the +5 state by the initial step in the standard procedure and was therefore not carried by the +5 niobium carrier. To surmount this difficulty, the irradiated thorium was dissolved in a 9:1 mixture of conc. HF and conc. HNO_3. This acid mixture easily dissolved Nb metal or NbO_2 and oxidized them both to the +5 state [18]. The solution was then made basic ($pH \sim 9$) with aqueous NH_3 to precipitate $Nb_2O_5 \cdot xH_2O$.

High-resolution gamma spectrometry was used to identify fission products and determine fission yields. The

detectors used to obtain the gamma spectra were a Canberra Ge(Li) detector with a 2.3-MeV resolution for the 1.33-MeV gamma ray from ^{60}Co and a 16% efficiency, two Ortec Ge(Li) detectors with a 2.1-keV resolution and a 15% efficiency, and an Ortec intrinsic Ge detector with a 1.75-keV resolution and 25% efficiency.

The gamma spectral data were reduced by the computer code HYPERMET [20]. A point source efficiency calibration was measured for a wide range of gamma energies using an Amersham mixed-source standard. Corrections to the point source efficiency calibration for the finite geometry of the sample and detector active volume were obtained from a computer simulation of the detector-sample system [21]. The resulting computer program was very similar to one devised by Moens *et al.* [22]. Activities of the various gamma-ray photopeaks, as determined by the HYPERMET analysis, were corrected for coincidence summing losses [23].

The areas found for the individual photopeaks in the gamma spectra were used to calculate the actual number of product atoms for a particular nuclide at the end of the irradiation, N_0. In the case of the independent yields, N_0 was determined by the standard relationship.

$$N_0 = \frac{SA}{F\varepsilon C(e^{-\lambda t_1} - e^{-\lambda t_2})} , \quad (1)$$

where A is the area of the photopeak, S is the summing coincidence correction, F is the fractional gamma-ray abundance, ε is the efficiency of the detector at the energy of the photopeak, C is a factor for the chemical yield in the radiochemical procedure, λ is the decay constant of the nuclide in question, and t_1 and t_2 are the times between the end of the irradiation and the beginning and end of the count, respectively. For the mass yields of ^{125}Sb and ^{127}Sb, N_0 was multiplied by a correction factor to account for the fraction of the total mass yield that came from the precursors at the time these precursors were separated from Sb during the radiochemical procedure. The rate of production for a particular nuclide during the irradiation, R, was determined by the relationship

$$R = N_0\lambda/(1 - e^{-\lambda t}) , \quad (2)$$

where t is the length of the irradiation. Yields of products were determined by comparing their rates of production during the irradiation to the rate of production for ^{140}Ba and multiplying by the mass 140 yield of 7.81% [6].

Fluctuations in peak bremsstrahlung energies during the irradiations were about ± 1 MeV. Since the half-lives of all of the fission products were long compared to the length of the irradiation, the energy fluctuations caused negligible effects in yields. Under similar irradiation conditions, an upper limit of 0.5% had been found for the contribution to the fission yields from neutron-induced fission resulting from neutrons produced by the photonuclear reaction ^{232}Th(γ,n) ^{231}Th [6].

A Fortran IV computer program was written to perform the statistical-dynamic model calculations [21].

III. RESULTS AND DISCUSSION

A. Experimental results

Independent yields for ^{82}Br, ^{96}Nb, ^{124}Sb^g, ^{126}Sb^g, and ^{136}Cs and upper limits for ^{86}Rb and ^{134}Cs were determined along with mass chain yields for masses 125 and 127 from irradiations at 27-MeV peak bremsstrahlung. The independent yield for ^{136}Cs was also determined at 15- and 11-MeV peak bremsstrahlung.

The fractional independent yields, shown in Table I were estimated using the mass yields determined by Hogan *et al.* [6]. The mass yields for masses 125 and 127 found in the present investigation were based on the assumption that the cumulative chain yields of ^{125}Sb and ^{127}Sb, respectively, represented the mass yields. The Z_p model FIY systematics indicated that the fraction of the chain yield for elements beyond Sb was negligibly small for masses 125 and 127. A plot showing the fit of these two mass yields with those of Hogan *et al.* [6] is shown in Fig. 1.

B. Z_p model

The Z_p model is based on the idea that the charge distribution of fission products for a given mass number will have a Gaussian shape with peak at the most probable charge, Z_p. The FIY is given by

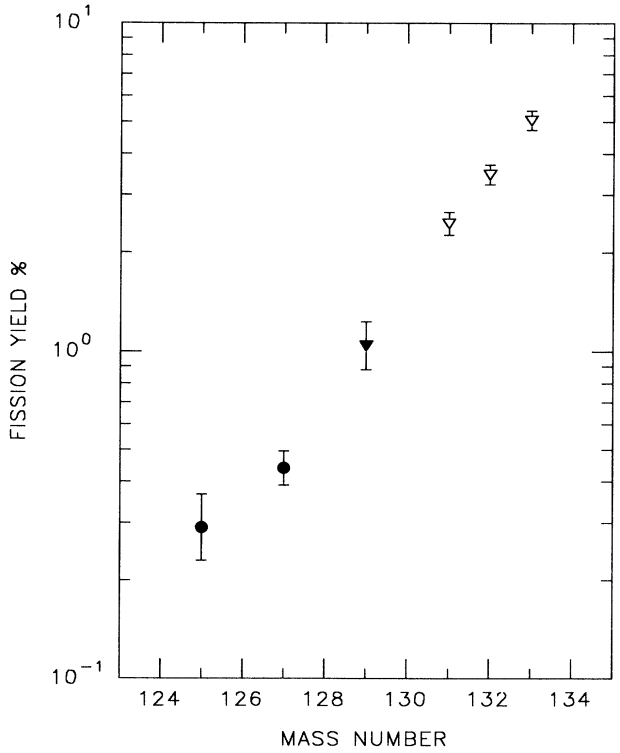

FIG. 1. Fission yields from photofission of ^{232}Th for this work and Hogan *et al.* [6] at comparable peak bremsstrahlung. This work at 27 MeV, ●; Hogan *et al.* [6] at 38 MeV, ▼; Hogan *et al.* [6] averaged between 15 and 38 MeV, ▽.

$$FIY = f_{eo}(\pi c)^{-1/2}\exp[-(Z-Z_p)^2/c] , \quad (3)$$

where f_{eo} is the even-odd effect factor and Z the charge for a particular nuclide in the mass chain. In an earlier investigation [24], the width parameter c for the charge distribution from the neutron-induced fission of ^{232}Th was found to be 0.71. Since the value of c should be nearly constant with changing excitation energy for low excitation fission [2], the value of 0.71 has been extended to ^{232}Th photofission in the present investigation.

Several methods have been developed to predict Z_p for various modes of fission. The unchanged-charge-distribution (UCD) method postulates that the neutron-proton ratio of the fissioning nucleus is unchanged in the fragments at scission [11]. The equal-charge-displacement (ECD) method postulates that the most probable charges of complementary fission fragments are equidistant from beta stability [12]. The minimum-potential-energy (MPE) postulate assumes that the charge division will be that which minimizes the nuclear potential energy [13]. The Nethaway empirical approach is a least-squares technique to correlate all fractional chain yields using thermal neutron fission of ^{235}U as a reference [14]. An even-Z enhancement and odd-Z depression factor of 1.30 was used for all four methods for predicting Z_p. The previous applications of these methods were summarized in an earlier paper [6].

A comparison of the experimentally determined and calculated FIY's is given in Table II. The good agreement in the asymmetric region probably reflects the fact that the Z_p model systematics were developed using experimental data heavy in asymmetric FIY's [14,25]. The rather poor agreement in the symmetric region is at least partly due to large uncertainties in $\bar{\nu}$, the average number of neutrons emitted per fragment of a particular mass and initial excitation energy [26]. The value of $\bar{\nu}$ also changes very rapidly at the nuclear temperature for which the stable, spherical shape of the 82-neutron shell starts to deform [27]. This nuclear temperature corresponds to an initial excitation energy of about 15 MeV for ^{232}Th.

The best fit to the experimentally determined FIY's in the present investigation is shown as the solid line in Fig. 2 and is compared with the values obtained by the various calculational methods. In general, there is good correlation between the experimental and calculated yields in the asymmetric region. The semiempirical mass binding-energy formula used to determine the ECD values does not follow the general trends of the other three methods. The fit of the two Sb isotopes, both in the symmetric region, would be good if the curve were shifted about $0.6Z_p$ units. This upward shift of Z_p in the

TABLE I. Independent, mass, and fractional independent yields measured for photofission of ^{232}Th at 27 MeV and other peak bremsstrahlung.

Nuclide	Independent yield (%) Present work[a]	Cunninghame[b]	Mass Yield (%)	FIY
^{82}Br	$(8.91\pm1.18)\times10^{-5}$	9.7×10^{-5}	0.61[c]	$(1.46\pm0.24)\times10^{-4}$
^{86}Rb	$<5.84\times10^{-4}$		6.35[c]	$<9.20\times10^{-5}$
^{96}Nb	$(2.40\pm0.36)\times10^{-5}$	2.8×10^{-5}	4.60[c]	$(5.22\pm0.94)\times10^{-6}$
^{124}Sb	$(1.26\pm0.15)\times10^{-3}$		0.4[d]	$(3.15\pm1.9)\times10^{-3}$
^{126}Sb	$(2.41\pm0.25)\times10^{-2}$		0.36[d]	$(1.17\pm0.34)\times10^{-1}$
^{134}Cs	$<1.42\times10^{-4}$		6.46[e]	$<2.20\times10^{-5}$
^{136}Cs	$(1.13\pm0.12)\times10^{-2}$	5.3×10^{-3}	6.85[c]	$(1.65\pm0.24)\times10^{-3}$
^{136}Cs[f]	$(3.37\pm0.36)\times10^{-3}$		6.05[g]	$(5.57\pm0.82)\times10^{-4}$
^{136}Cs[h]	$(1.06\pm0.14)\times10^{-3}$		5.68[i]	$(1.87\pm0.31)\times10^{-4}$

Mass	Cumulative Chain yield (%) Present work (27 MeV)	Mass yield Correction factor	Mass yield (%) Present work (27 MeV)
125	0.29±0.06	1.000	0.29±0.06
127	0.44±0.05	1.001	0.44±0.05

[a]27-MeV peak bremsstrahlung except as otherwise indicated.
[b]Cunninghame *et al.* (Ref. 10) at 23 MeV.
[c]Estimated by extrapolation or interpolation from values in Hogan *et al.* (Ref. 6) at 38 MeV.
[d]Estimated from masses 125 and 127 determined in the present work.
[e]From Hogan *et al.* (Ref. 6) at 38 MeV.
[f]15-MeV peak bremsstrahlung.
[g]Estimated by interpolation between masses 135 and 138 for 15-MeV peak bremsstrahlung from Hogan *et al.* (Ref. 6).
[h]11-MeV peak bremsstrahlung.
[i]Estimated by interpolation between masses 135 and 138 for 9-MeV peak bremsstrahlung from Hogan *et al.* (Ref. 6).

TABLE II. Experimental and Z_p model calculated FIY's for photofission of ^{232}Th at 27-MeV and other peak bremsstrahlung (unless indicated otherwise).

Nuclide	Expt.[a]	Nethaway[b]	UCD	ECD	MPE
^{82}Br	1.46×10^{-4}	1.97×10^{-4}	1.09×10^{-5}	3.82×10^{-5}	1.15×10^{-3}
^{86}Rb	$<9.20\times10^{-5}$	1.55×10^{-5}	4.46×10^{-7}	1.76×10^{-6}	6.28×10^{-5}
^{96}Nb	5.22×10^{-6}	2.16×10^{-5}	7.12×10^{-7}	2.28×10^{-6}	2.56×10^{-5}
^{124}Sb	3.15×10^{-3}	4.88×10^{-5}	7.63×10^{-4}	8.15×10^{-4}	2.62×10^{-4}
^{126}Sb	1.17×10^{-1}	2.21×10^{-5}	3.43×10^{-2}	3.52×10^{-2}	1.41×10^{-2}
^{134}Cs	$<2.20\times10^{-5}$	5.02×10^{-6}	2.71×10^{-4}	2.10×10^{-4}	1.85×10^{-5}
^{136}Cs	1.65×10^{-3}	1.32×10^{-3}	2.13×10^{-2}	1.84×10^{-2}	2.93×10^{-3}
^{136}Cs[c]	5.57×10^{-4}	7.88×10^{-4}	1.47×10^{-2}	1.10×10^{-2}	1.50×10^{-3}
^{136}Cs[d]	1.87×10^{-4}	4.04×10^{-4}	8.39×10^{-3}	5.79×10^{-3}	6.94×10^{-4}

[a]Experimental values this work.
[b]Nethaway empirical method.
[c]15-MeV peak bremsstrahlung.
[d]11-MeV peak bremsstrahlung.

symmetric region has also been observed in the photofission of ^{235}U and ^{238}U [3].

Several comparisons of Z_p's at different fragment masses with those found by the UCD method are shown in Fig. 3. Experimental data obtained in the present work are shown as plotted points while the values for the MPE, ECD, and Nethaway (NETH) methods are shown as solid lines. The experimental Z_p's fall in the generally predicted area for the asymmetric fragments. $A' \geq 131$ and $A' \leq 101$ (A' denotes the fragment mass prior to the neutron evaporation stage). However, the Z_p's for the two Sb isotopes, which are in the symmetric region, are shifted upward by about $0.6Z_p$ units from the values predicted by the models.

The determination of an accurate Z_p requires an accurate calculation of $\bar{\nu}$. The orthodox manner used to calculate $\bar{\nu}$ is to assume that, for any given fission pair, the total number of emitted neutrons, $\bar{\nu}_T$, is nearly constant and is given by the relation

$$\bar{\nu}_T = \bar{\nu}_H + \bar{\nu}_L \ , \tag{4}$$

where $\bar{\nu}_H$ and $\bar{\nu}_L$ are the average number of neutrons emitted for heavy and light fragments, respectively. This has been found to be a good approximation in the asymmetric region [25]. It has often been assumed that Eq. (4) also holds true in the symmetric region, and $\bar{\nu}_T$ is the

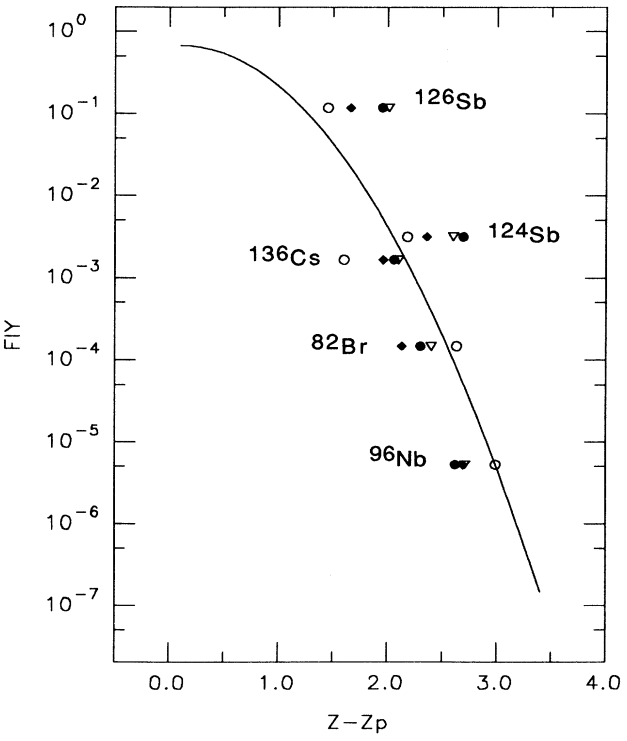

FIG. 2. Comparison of $Z - Z_p$ values for specific FIY's calculated using the MPE, ◆; ECD, ○; UCD, ●; and Nethaway, ▽, methods to the experimentally determined values (solid curve).

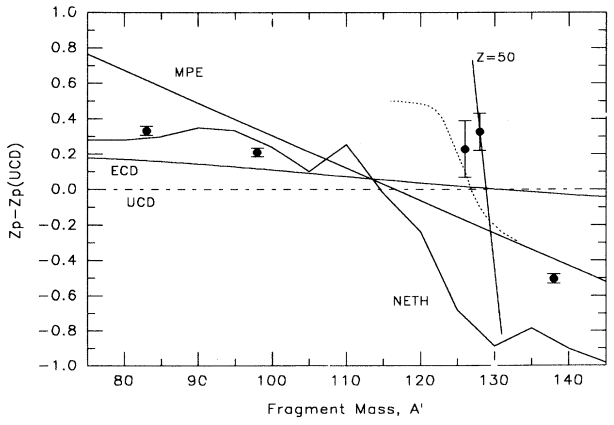

FIG. 3. Comparison of Z_p's at different fragment masses to those found by the UCD method. The dotted curve shows the deviation from the MPE method when the extra energy to increase $\bar{\nu}_T$ for symmetric fission is accounted for.

same in both regions. However, Wahl [25] reported that these assumptions do not give a good fit in the symmetric region.

The Coulombic repulsion between the symmetric fragments at scission is smaller than that for asymmetric fragments because of the more deformed and elongated shape of symmetric fragments [2,28]. As a result, there is less kinetic energy of the fragments for symmetric fission. Since the total energy released in the fission is nearly the same in both asymmetric and symmetric fission [29], there is greater energy available for emission of neutrons from fission fragments in symmetric fission, and this leads to a larger $\bar{\nu}_T$ for symmetric than for asymmetric fission. The energy available to produce $\bar{\nu}_T$ was calculated as the difference between the energy released in the fission [29] and the energy resulting in the kinetic energy of the fragments [30]. The energy available for neutron emission was divided by 6.3 MeV of excitation energy lost per emitted neutron to obtain $\bar{\nu}_T$ [2,8,31]. The value of $\bar{\nu}_T$ was found to be nearly constant at 3.1 ± 0.3 in the asymmetric region and 5.3 ± 0.3 in symmetric region. This increase of 2.2 extra neutrons emitted after scission translates into an increase of about $(0.5\pm0.1)Z_p$ units in Fig. 3. The dotted curve in Fig. 3 shows the deviation from the MPE method which results when the extra energy available to increase $\bar{\nu}_T$ for symmetric fission is taken into account. The experimental results for the photofission of ^{235}U and ^{238}U [3] are in good agreement with the dotted curve in Fig. 3.

C. Statistical-dynamic model

The recent availability of accurate ground-state masses for fissioning nuclei and fission fragments [29] has made possible the use of Fong's statistical theory of nuclear fission [15] to calculate FIY's. These calculations make use of the densities of quantum states of the fission fragments and the energy available to the fission system at scission. The density of quantum states $W_0(E)$ determines the relative probability of formation of a given fission fragment pair. The density of quantum states is determined by the excitation energy E of the nuclear system [32] and at any given time is given by

$$W_0(E)\propto a^{-1/4}E^{-5/4}\exp(2a^{1/2}E^{1/2}) . \quad (5)$$

The level density parameter a is usually determined experimentally as a function of the mass of nucleus [33,34].

According to Fong [15] the total amount of excitation energy available to the fission system at scission is given by the following equation:

$$E(A,Z)=M^*(A,Z)-M(A_1,Z_1)-M(A_2,Z_2) -K(A_1,Z_1,A_2,Z_2)-D(A_1,A_2) , \quad (6)$$

where $M^*(A,Z)$ is the ground-state mass of the fissioning nucleus plus any excitation energy. The terms $M(A_1,Z_1)$ and $M(A_2,Z_2)$ are the ground-state masses of the fragments formed at scission. The term $K(A_1,Z_1,A_2,Z_2)$ is the total kinetic energy of the fragments after they have reached their full Coulombic accelerated velocities and is a measure of the amount of Coulombic potential energy at the point of scission. The kinetic energies of the fragments were obtained from experimental data for neutron-induced fission of ^{232}Th [30]. This is justified, since the kinetic energies for both bremsstrahlung- and neutron-induced fissions of ^{232}Th are expected to be the same [2]. The term $D(A_1,A_2)$ is the total deformation energy of the fragments at scission. Deformation energies were approximated using the sawtooth curves of the average number of neutrons emitted, $\bar{\nu}$, vs fragment mass for the fission of ^{233}U [27,35]. The dependence of $D(A_1,A_2)$ on the charge of the fragments, for a constant mass, is small and can be neglected in most cases [15].

We have combined Fong's ideas [15] and post-fission dynamics to develop the statistical-dynamic method for calculating FIY's.

The probability for formation of a given fragment pair at scission is equal to its relative probability, as given by Eq. (5), divided by the sum of the relative probabilities of all possible fragment pair combinations:

$$P(Z_1,A_1,Z_2,A_2)=\frac{a_i^{-1/4}E_i^{-5/4}\exp(2a_i^{1/2}E_i^{1/2})}{\sum_j a_j^{-1/4}E_j^{-5/4}\exp(2a_j^{1/2}E_j^{1/2})} . \quad (7)$$

Correcting the respective A values in the equation for the number of post-fission neutrons then gives FIY's which can be used to construct the charge-distribution curve.

The number of post-fission neutrons evaporated from a particular fragment depends upon the sum of the excitation and deformation energies of the fragment. The thermal excitation energy of each fragment was determined by assuming thermal equilibrium at scission and then apportioning the total thermal excitation energy between the fragments in direct proportion to their masses. The deformation energy for each fragment was approximated and added to its thermal excitation. The sum of the excitation and deformation energies must be greater than the neutron binding energy for evaporation to occur. The binding energy of each neutron can be calculated from the ground-state masses of fission fragments [30]. Whenever a neutron is evaporated, the excitation energy is diminished by the neutron binding energy and the thermal energy of the neutron. The average thermal energy of the neutron can be approximated from the temperature of the fragment [2]. When the excitation energy for the fragment drops below the neutron binding energy, no more neutrons will be lost. Correcting for post-fission neutrons produces the pairing and shell effects which have been observed for the FIY's calculated with the statistical-dynamic model.

The computer program written to perform the statistical-dynamic model calculations was designed to follow the dynamics of the fission process starting with the assumption of statistical equilibrium just prior to scission and then following the post-fission phenomena as described above [21]. The statistical-dynamic calculation was integrated over the entire spectrum of bremsstrahlung energies using the cross-sections for first- and second-chance fission [8,9].

The accuracy of the method is very sensitive to the values of the ground-state masses. Accurate calculation of ground-state masses of fission-fragment nuclei is important because these nuclides are typically unstable and very short-lived, making experimental measurements difficult. A tabulation of such masses has recently become available [29].

Results of the statistical-dynamic calculations along with experimental FIY's are shown in Table III and Figs. 4(a)–(g). The solid lines in Figs. 4(a)–(g) are the Z_p Gaussian curves with c equal to 0.71 which have been placed to give the best agreement with the statistical-dynamic Z_p's shown in Table III.

The FIY's calculated by the statistical-dynamic model without proximity proton transfer are not shown, but they showed a general Gaussian shape which was somewhat narrower than that seen experimentally. This behavior has been true for other statistical calculations [15,36] and has been cited as a weakness of the statistical model. In Fong's statistical model, the width of the distribution is dependent solely upon the nuclear temperature [15].

Conventionally, the charge distribution has been assumed to have a Gaussian shape as represented by Eq. (3). This assumption was tested in an earlier investigation designed to look at the shape of the distribution on its wings [37]. The results of that investigation indicated that the distribution on a log-linear plot became approximately linear about one charge unit away from Z_p but no attempt was made to explain these results. One possible explanation involves proton transfer after scission. The idea that a proton has a small but finite probability of transfer after scission comes from proximity transfer reactions in heavy-ion collision reaction studies [38–45]. The results of the statistical-dynamic model calculations with proximity proton transfer are shown in Figs. 4(a)–(g). The linear behavior on the wings was shown for all the fission products calculated here. A probability for proton transfer after scission of 0.003 was used, and this produced very good agreement between calculated and experimental FIY's in all cases as seen in Figs. 4(a)–(g). The error in ground-state masses was estimated by Möller and Nix [29] to be ±0.8 MeV. Using a typical level density parameter of 20 MeV^{-1} and a typical excitation energy at scission of 22 MeV, the variance in the calculated FIY's resulting from the error in ground-state masses was found to be plus or minus a factor of 2.8 which corresponds to +180% and −64% in calculated FIY's. Other potential sources of error in the statistical-dynamic calculations were found to be relatively small.

TABLE III. Pairing effects calculated by the statistical-dynamic model for photofission of ^{232}Th with 27-MeV and other peak bremsstrahlung. All from 27-MeV peak bremsstrahlung except as otherwise indicated.

Mass number A	$Z_p b$[a]	Z	Gaussian FIY[b]	Statistical-dynamic FIY	Percent deviation	Average pairing effect, %
82	32.7	32	0.336	0.364	+8.3	
		33	0.590	0.589	−0.2	
		34	0.062	0.043	−31.1	−7.5
96	38.1	37	0.122	0.064	−47.2	
		38	0.660	0.824	+24.8	
		39	0.214	0.110	−48.6	+40.2
124	49.1	48	0.122	0.135	+10.7	
		49	0.660	0.509	−22.9	
		50	0.214	0.352	+64.5	+32.7
126	49.9	49	0.214	0.127	−40.6	
		50	0.660	0.757	+14.7	
		51	0.122	0.115	−5.7	+20.3
136	53.1	52	0.122	0.187	+53.4	
		53	0.660	0.073	−89.0	
		54	0.214	0.737	+244.9	+128.9
136[c]	52.7	52	0.336	0.399	+18.8	
		53	0.590	0.537	−9.0	
		54	0.062	0.058	−5.6	+7.4
136[d]	52.8	52	0.272	0.327	+20.2	
		53	0.633	0.560	−11.5	
		54	0.088	0.109	−23.9	+18.5
			Average without $A = 136$			+21.1±21[e]

[a]As determined by estimating the best fit of the statistical-dynamic FIY's to the Gaussian FIY's.
[b]With width parameter, c, of 0.71.
[c]15-MeV peak bremsstrahlung.
[d]11-MeV peak bremsstrahlung.
[e]The error shown is the replicate standard deviation of the averaged four values.

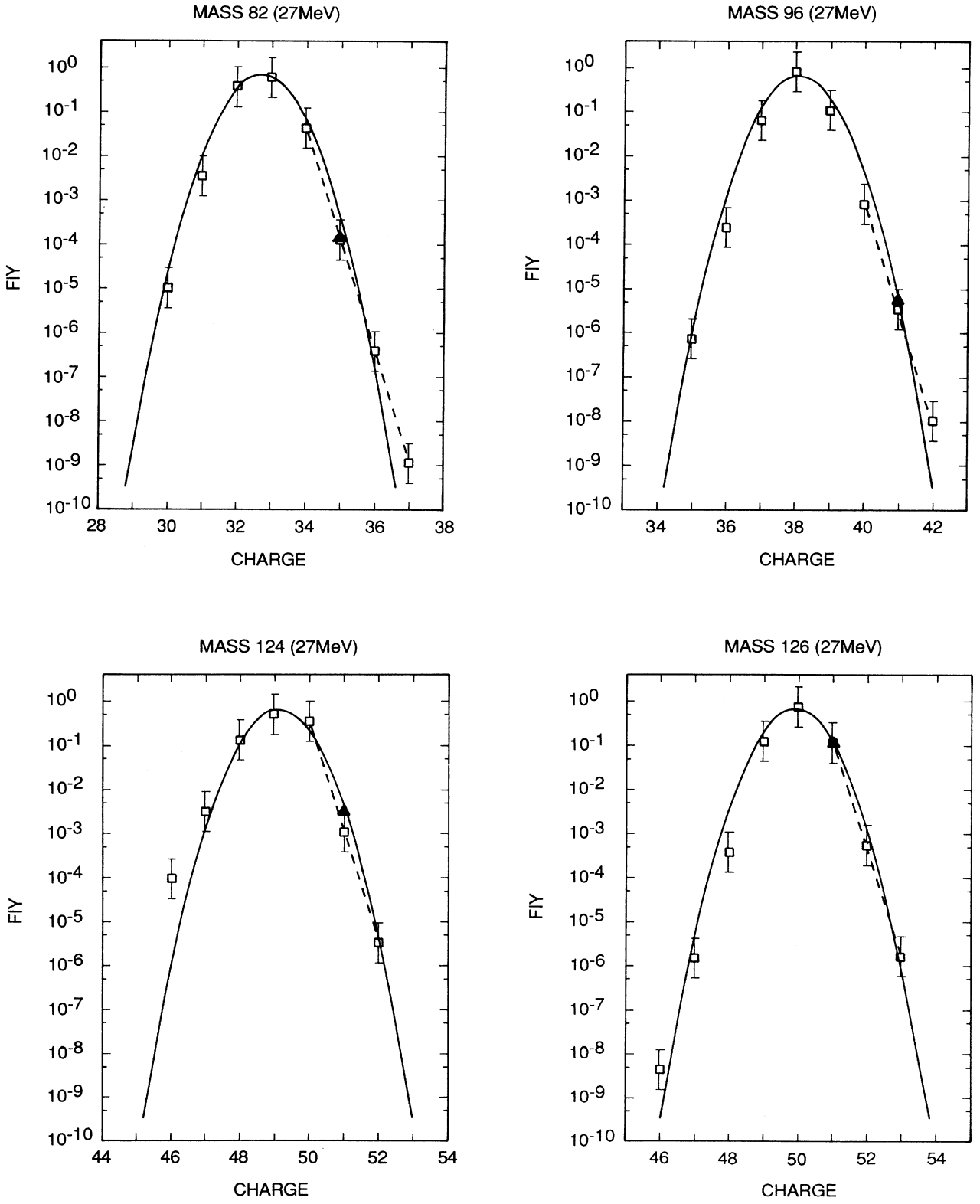

FIG. 4. (a)–(g) Statistical-dynamic model FIY's for charge distributions at different masses compared to those predicted by the Z_p model (solid curve) and those experimentally determined in this work, ▲; statistical-dynamic model calculation with proximity proton transfer, □. The dashed lines shows the linearity produced when proximity proton transfer is incorporated in the statistical-dynamic model calculation.

Another powerful capability of the statistical-dynamic model is its ability to produce pairing effects naturally. Experimental results from the fast neutron fission of ^{232}Th gave a net pairing effect of $+(30\pm12)\%$ for an even number of protons and $-(30\pm12)\%$ for an odd number of protons [46]. The demonstration of pairing effects from the statistical-dynamic calculations can be seen in Figs. 4(a)–(g). The magnitudes of the pairing effects for

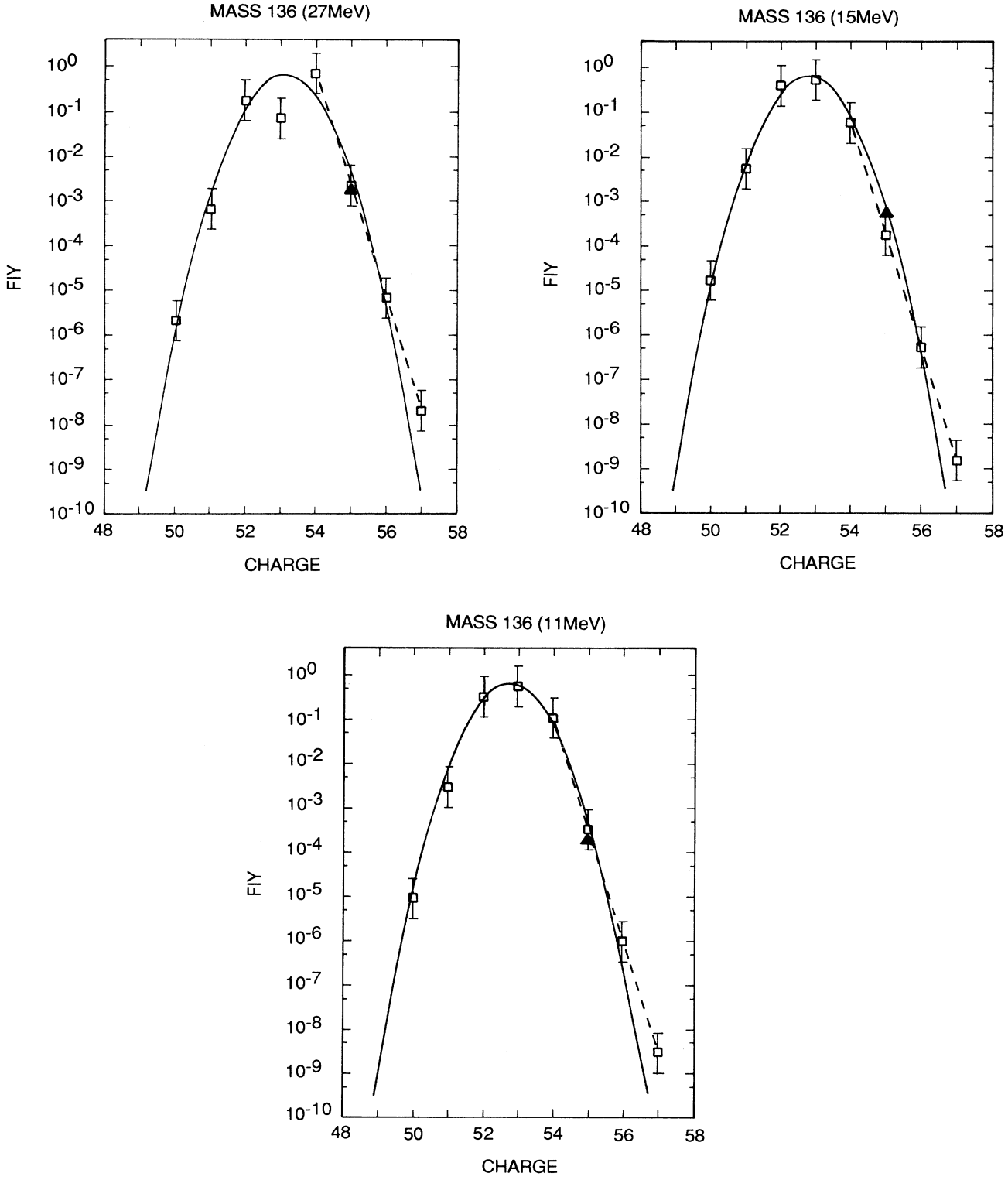

FIG. 4. (*Continued*).

each of the fission products investigated here are shown in Table III as percentage differences of calculated FIY's from the Z_p Gaussian curves for the three largest FIY's for each mass number. The three pairing effect values for each possible fission product sum together to give a net effect for the mass number. If the observed pairing effect is negative for an even number of protons or positive for an odd number of protons, it is listed as a negative percentage in the table.

The error limits for the FIY's shown in Table III are smaller than those for the corresponding points in Figs. 4(a)–(g) for several reasons. The root-mean-square error in the calculated ground-state masses within a small range of masses and charges is usually smaller than the full root-mean-square error of ±0.8 MeV [29]. The variance in the calculated versus experimental ground-state masses for three consecutive charges, each with the same mass number, is typically only about ±0.3 MeV. This error translates into an error in the calculated FIY's of only about +45% and −31%, much less than the +180% and −64% for the entire curve. With this smaller error it is possible to see pairing effects as small as ±20% at the top of the charge-distribution curve. The average pairing effect for the charge-distribution curves for masses 82, 96, 124, and 126 was found to be (21±21)% and is in good agreement with the pairing effects of (30±12)% observed in the earlier work [46]. The pairing effects for mass 136 were not included in the above average because of the likelihood of large errors in calculated FIY's at mass 136. Large deviations in calculated FIY's such as are seen for mass 136 at 27 MeV are likely due to errors in ground-state mass calculations in the region near the 82 neutron shell [29]. No other major sources of error for calculated pairing effects were found. For example, they were little affected by changes in the width parameter, c and in Z_p.

According to Fong's original statistical model [15], the pairing effects should occur over the entire charge-distribution curve. This has also been assumed in the Z_p model calculations, but Shmid *et al.* [37], who observed the wing effect discussed above, saw a strong pairing effect for $Z-Z_p \leq 1$, but only a slight, if any, pairing effect for $Z-Z_p > 1$. This is in complete agreement with the results of the statistical-dynamic model with proximity proton transfer which not only produced the wing effect but also washed out the pairing effects on the wings of the distribution where $Z-Z_p > 1$. Shmid *et al.* [37] did not comment on what is apparent from their data, that the pairing effect was lost on the wings.

The statistical-dynamic model also produces shell effects naturally. There are two types of shell effects: (1) those produced at scission and (2) those produced during the post-scission neutron evaporation stage of the fission products.

According to Izak-Biran and Amiel [42], shell effects at scission caused by neutron shells are mostly washed out during neutron-induced fission of ^{232}Th. In addition, the present statistical-dynamic calculations produce no noticeable 50-proton shell effects. Deviations of Z_p in the symmetric region have, at times, been attributed to the influence of the 50-proton shell (see Fig. 3) [47]. This proton number is also associated with masses around 132, so the deviations in Z_p may also be due to the 82-neutron shell and its stabilizing effect on asymmetric fission.

Shell effects arising in the post-scission neutron evaporation state, typically for the 82-neutron shell, have been observed experimentally [46], but the enhancement of yields seen for some nuclei with 82 neutrons was not observed for others with 82 neutrons. The statistical-dynamic model shows this same appearance of a neutron-shell effect for some nuclei, but not for others.

IV. CONCLUSIONS

In general, both Z_p and statistical-dynamic models were successful in reproducing the experimentally determined FIY's within expected error limits in the asymmetric region, with $A \leq 100$ and ≥ 132. The Z_p model was less satisfactory in the symmetric region because of uncertainties of $\bar{\nu}$ values in that region. An advantage of the statistical-dynamic model is that it is not limited by the quality and number of experimental FIY's. The accuracy of the FIY's from the statistical-dynamic model is limited only by the correctness of the model and the input values, most importantly, the ground-state masses. As the input values become more accurate, the calculated FIY's will become more accurate.

Another advantage of the statistical-dynamic model is its potential as a theoretical tool to better understand the dynamics of the fission process. The statistical-dynamic model uses many of the characteristic quantities of the fission process, such as kinetic energies of the fragments and deformation energies at scission, as input data for calculating FIY's. Each step of the fission process can incorporate experimental or calculated values to test the validity of an idea, such as proximity proton transfer in this investigation, or reveal mechanisms that produce the characteristics of the fission process. The Z_p model, on the other hand, is less useful as a theoretical tool because its design, being primarily an empirical functional fit to the experimental data, gives little insight into the actual mechanisms which produce the results the model was designed to predict. Weaknesses include its total inability to predict, and only model, pairing and shell effects which are produced naturally by the statistical-dynamic model.

ACKNOWLEDGMENTS

The authors wish to thank Dr. J. L. Meason, Dr. W. W. Sallee, and Dr. M. Flanders of White Sands Missile Range for their help and suggestions. The support and assistance of the personnel of the Nuclear Effects Laboratory at WSMR is greatly appreciated, especially A. De La Paz who made this facility available and J. Borrett for his time and skill in operation of the LINAC. This work was supported in part (J.R.S.) by the Associated Western Universities–Department of Energy with the cooperation of the Nuclear Effects Laboratory at White Sands Missile Range, New Mexico.

*Present address: 1185 Norman Street, North Augusta, SC 29841.

†Present address: 2457 U 50 Road, Cedaredge, CO 81413.

[1] A. Bohr, in *Proceedings of the United Nations International Conference on the Peaceful Uses of Atomic Energy, Geneva, 1956* (United Nations, New York, 1963), Vol. 2, p. 151.

[2] R. Vandenbosch and J. R. Huizenga, Nuclear Fission (Academic, New York, 1973).

[3] D. D. Frenne, H. Thierens, B. Proot, E. Jacobs, P. D. Gelder, and A. De Clercq, Phys. Rev. C **26**, 1356 (1982).

[4] H. Thierens, B. Proot, D. De Frenne, and E. Jacobs, Phys. Rev. C **25**, 1546 (1982).

[5] P. D'hondt, E. Jacobs, A. De Clercq, D. De Frenne, H. Thierens, P. De Gelder, and A. D. J. Deruytter, Phys. Rev. C **21**, 963 (1980).

[6] J. C. Hogan, A. E. Richardson, J. L. Meason, and H. L. Wright, Phys. Rev. C **16**, 2296 (1977).

[7] W. Gunther, K. Huber, U. Kneissel, H. Krieger, and H. J. Maier, Z. Phys. A **295**, 333 (1980).

[8] J. T. Caldwell, E. J. Dowdy, B. L. Berman, R. A. Alvarez, and P. Meyer, Phys. Rev. C **21**, 1215 (1980).

[9] J. W. Knowles, W. F. Mills, and R. N. King, Phys. Lett. **116B**, 315 (1982).

[10] J. C. Cunninghame, M. P. Edwards, G. P. Kitt and K. H. Lokan, Nucl. Phys. **44**, 588 (1963).

[11] R. K. Gupta and D. R. Saroha, Phys. Rev. C **30**, 395 (1984).

[12] C. D. Coryell, M. Kaplan and R. D. Fink, Can. J. Chem. **39**, 646 (1961).

[13] W. J. Swiatecki, J. Phys. (Paris) Colloq. **33**, C5-45 (1972).

[14] D. R. Nethaway, Lawrence Livermore Laboratory Report No. UCRL-51640, 1974.

[15] P. Fong, *Statistical Theory of Nuclear Fission* (Gordon and Break, New York, 1969).

[16] R. S. Clark and J. N. Beck, *Radiochemical Procedures. The Fission Products* (Nuclear Group, University of Arkansas, 1975).

[17] J. Klienberg and H. L. Smith, Los Alamos Scientific Laboratory Report LA-1721, 1975.

[18] I. M. Gibalo, *Analytical Chemistry of Niobium and Tantalum* (Ann Arbor-Humphrey Science, London, 1970).

[19] D. I. Ryabchikov and E. K. Gol'braikh, *Analytical Chemistry of Thorium* (Ann Arbor-Humphrey Science, London, 1969).

[20] G. W. Phillips, Oak Ridge National Laboratory Report PSR-101/ HYPERMET, 1976.

[21] J. R. Smith, Ph. D. dissertation, New Mexico State University, 1986.

[22] L. Moens, J. De. Donder, Lin Xi-lei, F. De Corte, A. DeWispelaere, A. Simonits, and J. Hoste, Nucl. Instrum. Methods **187**, 451 (1981).

[23] K. Debertin and U. Schötzig, Nucl. Instrum. Methods **158**, 471 (1979).

[24] H. Erten, A. Grutter, E. Rossler, and H. von Gunten, Phys. Rev. C **25**, 2519 (1982).

[25] A. C. Wahl, J. Radioanal. Chem. **55**, 111 (1980).

[26] Y. Patin, S. Cierjacks, J. Lachkar, J. Sigaud, G. Haouat, and F. Cocu, Nucl. Instrum. Methods **160**, 471 (1979).

[27] C. J. Bishop, R. Vandenbosch, R. Aley, R. W. Shaw, Jr., and I. Halpern, Nucl. Phys. **A150**, 129 (1970).

[28] H. C. Britt, H. E. Wegner, and J. C. Gursky, Phys. Rev. **129**, 2239 (1963).

[29] P. Möller and J. R. Nix, At. Data Nucl. Data Tables **26**, 165 (1981).

[30] A. I. Sergachev, V. G. Vorob'eva, B. D. Kuzminov, V. B. Mikhailov, and M. Z. Tarasko, Yad. Fiz. **7**, 778 (1968) [Sov. J. Nucl. Phys. **7**, 475 (1968)].

[31] N. Bohr, Nature **137**, 344 (1936).

[32] J. R. Huizenga and L. G. Moretto, Annu. Rev. Nucl. Sci. **22**, 427 (1972).

[33] D. W. Lang, Nucl. Phys. **53**, 113 (1964).

[34] M. Barranco and J. Treiner, Nucl. Phys. **A351**, 269 (1981).

[35] F. Plasil, R. L. Ferguson, F. Pleasonton, and H. W. Schmitt, Phys. Rev. C **7**, **1186** (1973).

[36] U. Facchini and G. Sassi, J. Phys. G **3**, 269 (1977).

[37] M. Shmid, Y. Nir-el, G. Engler, and S. Amiel, J. Inorg. Nucl. Chem. **43**, 867 (1981).

[38] J. Randrup, Nucl. Phys. **A307**, 319 (1978).

[39] J. Randrup, Ann. Phys. **112**, 356 (1978).

[40] J. Randrup and W. J. Swiatecki, Nucl. Phys. **A429**, 105 (1984).

[41] F. Beck, M. Dworzecka, and H. Feldmeier, Z. Phys. A **289**, 113 (1978).

[42] S. Ayik, B. Schurmann, and W. Norenberg, Z. Phys. A **279**, 145 (1976).

[43] W. Norenberg, Phys. Lett. **53B**, 289 (1974).

[44] J. Blocki, Y. Boneh, J. R. Nix, J. Randrup, M. Robel, A. J. Sierk, and W. J. Swiatecki, Ann. Phys. **113**, 330 (1978).

[45] J. Randrup, Nucl. Phys. **A327**, 490 (1979).

[46] T. Izak-Biran and S. Amiel, Phys. Rev. C **16**, 266 (1977).

[47] A. C. Wahl, Phys. Rev. C **32**, 184 (1985).